Int. J. Heat Mass Transfer. Vol. 30, No. 10, pp. 2083–2095, 1987
Printed in Great Britain

0017–9310/87 $3.00 + 0.00

Boiling heat transfer and critical heat flux in liquid films falling on vertically-mounted heat sources

I. A. MUDAWWAR, T. A. INCROPERA and F. P. INCROPERA
Heat Transfer Laboratory, School of Mechanical Engineering, Purdue University, West Lafayette, IN 47907, U.S.A.

(*Received* 11 *September* 1986 *and in final form* 4 *March* 1987)

Abstract—Boiling heat transfer measurements were obtained for an inert fluorocarbon (FC-72) liquid film injected over a vertical heated wall. Flow visualization revealed that vigorous boiling prior to burnout ruptured the liquid continuum, causing most of the film to separate from the heated wall leaving a thin liquid subfilm which maintained contact with the wall. The critical heat flux (CHF) was accompanied by dryout of the subfilm after total separation of the liquid near the upstream edge of the heater. A higher CHF was achieved by increasing the film velocity or by utilizing a shorter heater. Experimental data correlated favorably with predictions of a CHF model based on the Helmholtz instability and subfilm dryout.

INTRODUCTION

A FUNDAMENTAL understanding of boiling heat transfer in thin liquid films is important to applications such as thin film evaporators, water-cooled turbine blades, nuclear fuel rods, and laser mirrors. Thin films are utilized in a variety of cooling configurations. Examples include horizontal stationary films, gravity-driven films, shear-driven (annular-flow) films, wall jets, and radial films formed by jet impingement.

According to Mesler [1], nucleate boiling in a thin liquid film reduces the wall superheat compared to pool boiling. This behavior was attributed to the short trajectory a bubble needs to traverse within a thin film before escaping at the free surface. The nucleation pattern contrasts sharply with that of pool boiling, where a bubble establishes a long trajectory along which it experiences considerable resistance by liquid inertia. Furthermore, the enormous growth of bubbles along trajectories in a liquid pool provides a resistance for liquid flow to the hot wall.

An important aspect of heat transfer enhancement in thin boiling films concerns microlayer evaporation. As a bubble grows in any boiling system, it tends to trap a thin liquid layer (microlayer) between the growing bubble and the heated wall. Since the thickness of this layer is typically of the order of 1 μm [2], it provides a highly conductive path for heat dissipated at the wall. This heat is rejected by evaporation of the microlayer surface. Microlayer evaporation is a major contributor to increasing the heat transfer coefficient associated with boiling [3, 4]. In pool boiling the contact time of the bubble with the surface is long enough for the microlayer to evaporate completely, and microlayer evaporation is nonexistent for a considerable fraction of the bubble history prior to detachment. In thin boiling films, on the other hand, bubbles detach from the hot wall before the microlayer has time to dryout. Therefore, microlayer evaporation is active over a larger fraction of the bubble contact time, and higher heat fluxes may be achieved for the same wall superheat.

Although microlayer evaporation may provide an explanation for nucleate boiling enhancement in thin stationary horizontal films, flowing films may exhibit different nucleation patterns due to the strong influence of liquid motion on the growing bubbles. Ueda *et al.* [5] indicated that bubbles growing within a low velocity, gravity-driven film burst directly through the film surface. Bubbles in high speed films, on the other hand, are dragged along with the liquid stream instead of growing and bursting at the active nucleation sites. Thus microlayer evaporation is very important near the upstream edge of the hot wall. Further downstream, the large void fraction within the film caused by entrainment of a large population of bubbles thickens the film significantly and endangers the existence of a liquid continuum near the hot wall. Thus the attractive nucleate boiling capabilities of high speed films deteriorate rapidly when employed with long heated surfaces.

The similarity of the CHF mechanism in most flowing film geometries (falling films, shear-driven films, wall jets, impinging jets) is evidenced by the optical studies and visual observations of several investigators [5–12]. In one such effort, Katto and Ishii [9] experimented with a liquid jet driven by a nozzle at an angle to the surface of a rectangular heater. They witnessed noticeable thickening of the boiling film in the flow direction due to the entrainment of bubbles by the jet. At higher heat fluxes the greater part of the liquid was driven from the hot wall by intense vapor

NOMENCLATURE

A	total heat transfer area
A_g	total cross-sectional area of vapor jets
c_{pf}	specific heat of liquid at constant pressure
C_{sub}	constant in equation (12)
C_λ	constant in equation (6)
g	acceleration due to gravity
h_{fg}	latent heat of vaporization
k_f	thermal conductivity of the saturated liquid
L	heater length
q	wall heat flux
q_M	critical heat flux (CHF)
T_{sat}	saturation temperature corresponding to the operating pressure
T_{sub}	subcooled temperature of the liquid
T_w	wall temperature
ΔT_{sat}	wall superheat
ΔT_{sub}	wall subcooling
U	average film speed
u_f	velocity of liquid normal to the hot wall
u_g	velocity of vapor normal to the hot wall.

Greek symbols

δ	nozzle spacing
δ_M	thickness of liquid subfilm
λ_H	critical wavelength for Helmholtz instability
μ_f	viscosity of the saturated liquid
μ_g	viscosity of the saturated vapor
ρ_f	density of the saturated liquid
ρ_g	density of the saturated vapor
σ	surface tension.

effusion, while a very thin liquid subfilm remained in contact with the wall. At CHF, the subfilm began to dryout near the downstream edge of the heated wall and a dry patch extended up towards the nozzle while the liquid was totally driven from the wall.

Monde and Katto [10] chose ten physical variables to correlate CHF data in saturated impinging jets and wall jets. These variables include the critical heat flux, q_M, the latent heat of vaporization, h_{fg}, the vapor and liquid densities, ρ_g and ρ_f, the vapor and liquid viscosities, μ_g and μ_f, the surface tension, σ, the buoyancy force normal to the boiling surface, $g_n(\rho_f-\rho_g)$, the characteristic velocity of the forced flow, U, and the heater length, L. Following the pi theorem, they developed a general CHF correlation based on six dimensionless groups

$$\frac{q_M/\rho_g h_{fg}}{U} = C\left(\frac{\rho_f}{\rho_g}\right)^{n_1}\left(\frac{\mu_g}{\mu_f}\right)^{n_2}\left(\frac{\sigma}{\rho_f U^2 L}\right)^{n_3}\left(\frac{\mu_f}{\rho_f U L}\right)^{n_4} \times\left(\frac{g_n(\rho_f-\rho_f)L}{\rho_f U^2}\right)^{n_5} \quad (1)$$

where C and the five exponents n_1 through n_5 are empirical constants. Monde and Katto assumed that gravity has no effect on CHF for horizontal surfaces or for high speed jet flow on smaller surfaces. In addition, they pointed out that fluid viscosity had little effect on the burnout heat flux for many ordinary fluids. Thus equation (1) was simplified to the form

$$\frac{q_M/\rho_g h_{fg}}{U} = C\left(\frac{\rho_f}{\rho_g}\right)^{n_1}\left(\frac{\sigma}{\rho_f U^2 L}\right)^{n_3} \quad (2)$$

where the term on the left-hand side represents the ratio of the 'superficial' vapor velocity normal to the boiling surface to the characteristic flow velocity. The second dimensionless group on the right-hand side is the reciprocal of the Weber number based on the heater length.

The dimensionless representation of equation (2) has been successful in correlating CHF data for falling films [5, 12], wall jets [6, 9, 12] and impinging jets [7, 8, 10, 11]. Nevertheless, these correlations were specific for the operating pressure range of the individual experimental studies. Katto and Shimizu [11], for example, conducted several jet impingement experiments on a circular heated disc. Water and Freon 113 were tested at atmospheric pressure, while high pressure experiments were conducted in the range from 6 to 27.9 bar using Freon 12. They correlated their data by two different equations which followed the dimensionless representation of equation (2). Yet each of the two correlations was unique to the operating pressure range.

Several attempts have been made to model the CHF mechanism in flowing liquid films. Lienhard and Eichhorn [13] explained Katto and Shimizu's [11] correlations for jet impingement on circular discs using Lienhard's well-known mechanical energy stability criterion, which was originally developed for cross-flow of saturated liquid over a horizontal cylindrical heater [14]. CHF was modeled by equating the kinetic energy of the vapor formed at the heater surface to the energy required to overcome surface tension forces responsible for maintaining the liquid continuum of the jet. Since little information was available concerning the size and distribution of the splashed droplets, Lienhard and Eichhorn introduced empirical constants to develop a single CHF correlation which applies for both pressure ranges of the Katto and Shimizu data.

Baines *et al.* [12] presented an alternative mechanistic model for CHF which applied for wall jets and falling films. They maintained that, even when the film separates from the hot wall during severe boiling, adequate cooling of the wall is still possible by droplets that are ejected from the separated film. As the heat flux is increased, the separation angle of the film will

also increase, ejecting droplets further downstream on the surface. CHF occurs when most of the droplets are ejected beyond the downstream edge of the heater.

Katto [15] presented a comprehensive review article on CHF models and correlations for pool and forced convection boiling, which included several studies on thin film boiling systems. The article discusses a CHF model developed earlier by Haramura and Katto [16] for saturated pool and forced convection boiling systems. The model is based on the assumption that, in the high heat flux nucleate boiling region, vapor jets leaving the boiling surface are rendered hydrodynamically unstable due to the Helmholtz instability and a large vapor blanket is formed at the heated wall. They postulated that cooling of the wall is limited by the supply of liquid to a thin liquid layer trapped between the blanket and the wall.

In this paper, data taken with Fluorinert FC-72 (product of 3M company) flowing films are reported. The study was conducted to assess the feasibility of using free-falling dielectric fluids to cool vertically mounted electronic chips. Results of extensive photographic studies which depict the mechanistic role of flow parameters on CHF are presented. A CHF model based on subfilm dryout is used as a basis for correlating the experimental data.

EXPERIMENTAL APPARATUS

The flow loop utilized in this study was designed to insure high purity circulation of the working fluid (FC-72) over the boiling surface. As shown in Fig. 1, the fluid was boiled inside a deaeration vessel prior to delivery into the primary flow loop. The deaeration vessel consisted of a 3 gallon stainless steel container fitted with four immersion heaters on its bottom section and a reflux condenser mounted directly above the vessel. Prior to testing, the primary flow loop was evacuated to less than 500 μm Hg to remove air and other noncondensible gases. The working fluid was then charged into the main reservoir, where it was stored for subsequent runs. During startup, the fluid was circulated within the primary loop by a stainless steel, magnetically-driven centrifugal pump, while being heated by a temperature-controlled electric heater. The operating pressure within the test chamber was monitored by an absolute pressure transducer, and the fluid flow rate was measured through a turbine flowmeter. A cyclone phase separator located downstream of the electric heater rejected all entrained vapor back into the reservoir, allowing only liquid to enter the test chamber. The separator eliminated flow rate measurement errors by the turbine flowmeter. A sight glass connected between the phase separator and the flowmeter facilitated visual observation of the fluid upstream of the flowmeter to insure bubble-free flow. The flow rate was controlled by varying the speed of the pump and bypassing some of the fluid into the reservoir. Steady-state pressure and temperature control were achieved by condensing the vapor produced in the test chamber and routing the condensate back into the reservoir, as well as by heating the fluid in the primary electric heater to balance heat losses from the loop. A secondary heat exchanger located upstream of the test chamber was also used in some runs to achieve subcooled film conditions.

The test chamber, which is shown in Fig. 1, consisted of two parts, the inner film injection chamber and the outer enclosure. Both chambers were fabricated of G-10 fiberglass and fitted with optical-grade polycarbonate (Zelux-W) windows to facilitate visual access to the boiling film. As shown in Fig. 2, the fluid was introduced into the inner chamber through a stainless manifold in crossflow over a cylindrical cartridge heater. This heater was utilized as a thermal guard against heat losses for saturated film data. The fluid was introduced over the vertical heated module via an adjustable rectangular nozzle. A vapor bleed line was located at the top of the inner chamber to vent any vapor before reaching the nozzle.

Four different rectangular heater modules were tested to correlate the length effect of CHF. The modules were 25.4 mm wide, with lengths of 12.7, 25.4, 63.5 and 127 mm. As shown in Fig. 3, each module consisted of three parallel attachments: an oxygen-free copper surface, a heat source, and an insulating substrate. The 5.1 mm thick copper plate provided a thermally conductive path from the heat source to the boiling film. The boiling surface was prepared with ultrafine 600 silicon carbide sandpaper and cleaned before each run with acetone. The heat source consisted of a nickel–chromium resistive wire, 0.356 mm in diameter, sandwiched between two thermally conducting boron nitride ceramic plates ($k = 65\,\mathrm{W\,m^{-1}\,K^{-1}}$). Fourteen vertical grooves, 0.28 mm deep and 0.406 mm wide, were machined in the surface of the boron nitride plate adjacent to the copper plate. The wire was placed within the grooves and covered with fine boron nitride powder to minimize thermal contact resistances. The G-7 fiberglass insulating substrate insured that most of the heater power was dissipated to the boiling surface and provided for careful alignment and secure mechanical clamping of the module. A two-dimensional numerical analysis of heat transfer within the module revealed that less than 10% of the input power is lost to the G-7 substrate.

The resistive wire was heated by a 300 V, 9 A d.c. Sorensen power supply. The heater voltage drop was measured across the power leads to the nichrome wire, while the current was measured across an external shunt connected in series with the heater. Differential thermocouples were employed to measure the temperature of the copper plate. One junction of each chromel–alumel thermocouple (0.125 mm diameter) was embedded within the copper plate 2.54 mm away from the boiling surface. The other junction was immersed in the fluid upstream of the nozzle. Thus the temperature of the copper block relative to the fluid temperature was measured accurately, even for

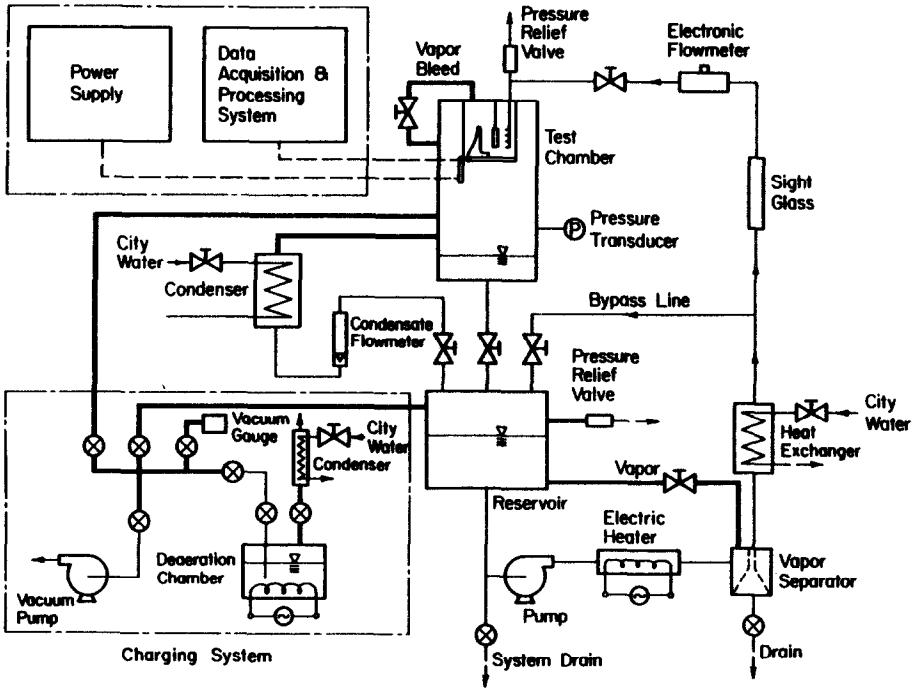

FIG. 1. Schematic diagram of the test facility.

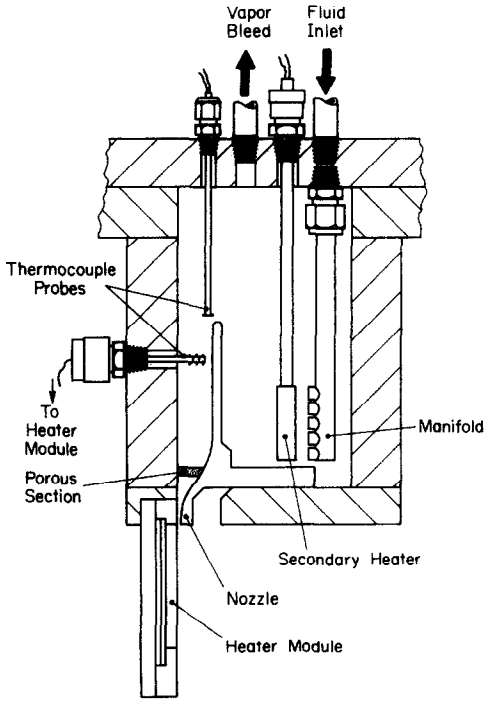

FIG. 2. Sectional diagram of the inner test chamber.

small degrees of superheat. The absolute temperature of the fluid was measured independently using a copper–constantan thermocouple. The heater module was protected against burnout by an electronic comparator circuit. The voltage signal of a thermocouple embedded within the copper plate was monitored relative to a prescribed reference voltage. When the copper plate overheated subsequent to CHF, the reference voltage was exceeded and the circuit triggered a relay which cut off power to the heater in less than 10 ms.

During operation, electric power to the heater module was increased gradually in small increments. When the temperature of the copper plate reached steady state, the flow rate, chamber pressure, inlet temperature, heater temperature and power level were read and stored by a HP (Hewlett Packard) 3054 data acquisition system. At this point the operator was prompted by a HP 9826 microcomputer to increase the power of the heater. This procedure was repeated until CHF was reached. At CHF the rapid rise in the heater temperature was detected by the protection circuit, which energized the power relay and cut off power to the module.

In addition to heat transfer measurements, detailed photographic studies were performed during most of the runs. The optical system consisted of a 35 mm camera equipped with a 35–105 mm zoom lens and a stroboscope light source. The stroboscope was synchronized for flash durations in the range from 0.8 to 30 μs to capture the rapid motion of discrete bubbles and droplets in the boiling film.

VISUAL OBSERVATIONS AND OPTICAL STUDIES OF THE BOILING FILM

To determine the effect of increasing heat flux on film development, flow visualization was performed

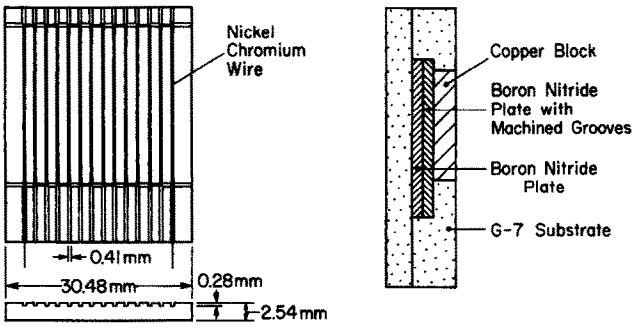

FIG. 3. Construction of the test heater.

during most of the tests. These studies were used to identify the mechanistic role of individual parameters on the boiling process, particularly near CHF. The matrix of operating conditions for each of the four heaters consisted of four nozzle spacings ($\delta = 0.25$, 0.50, 1.00 and 1.50 mm) and four inlet velocities ($U = 0.50$, 1.00, 1.50 and 2.00 m s^{-1}). Data were obtained with FC-72 at atmospheric pressure ($T_{sat} = 56°C$), and film subcooling for most of the experiments was limited to $\Delta T_{sub} < 6°C$, with the largest subcooling corresponding to the 63.5 and 127.0 mm long heaters.

The development of nucleate boiling was similar for each test, except near burnout, where major differences in film behavior were observed near the downstream end of the different heaters. The onset of nucleate boiling was evidenced by the activation of a few cavities near the downstream edge of the heater. An increase in the wall heat flux increased the number of active sites in both the spanwise and upstream directions. The surface of the heater was marked with longitudinal nucleation 'streams', each of which emanated from a single upstream active site. Higher fluxes created more nucleation streams in the spanwise direction and moved the front of the streams closer to the nozzle. This stage of film development occurred after a small increase in power beyond the onset of nucleation.

Figure 4 shows front views of the film during successive stages of boiling leading to burnout. These pictures were obtained for a film thickness of $\delta = 0.50$ mm and a velocity of $U = 0.60$ m s^{-1}, using the 63.5 mm long heater. Figure 4(1) shows the bare copper surface, prior to film injection, flush-mounted in the white G-7 fiberglass substrate. The threaded holes on each side of the surface were used in some tests for side-wall attachments. Figure 4(2) shows the individual nucleation streams obtained at 36% of CHF. In Fig. 4(3) more nucleation streams are visible near the mouth of the nozzle. The individual streams thicken in the flow direction and merge with other streams, forming a fairly homogeneous two-phase mixture. At 69% of CHF, Fig. 5(4), nucleation sites completely span the upstream edge of the heater, while nucleation streams are no longer clearly discernible. Due to excessive bubble entrainment, the void ratio on downstream sections of the heater became too large for the film to maintain a liquid continuum. Smaller bubbles seem to coalesce into much larger bubbles, which interrupt the film motion and break it into individual droplets and liquid streamers. The destructive role of the large bubbles is encountered at fluxes as low as 69% of CHF, and is noticeable over most of the heater length just prior to CHF, Figs. 4(5)–(7).

Partial dryout also occurs near the sides of the heater, especially at the downstream edge where the broken streamers show signs of convergence towards the central region. Figure 4(8) depicts the film soon after CHF. A few nucleation sites, still visible at the upstream edge of the heater, seem to generate enough bubbles to separate the film by venting all the vapor between the separated liquid and the wall. Since it is impossible to set the heater power at exactly the level which triggers CHF, Figs. 4(7) and (8) correspond to conditions which precede and succeed CHF, respectively. Thus, CHF was assumed to correspond to 50% of the last power increment beyond the heat flux of Fig. 5(7). At 99% of CHF, a very thin subfilm was observed by the naked eye to maintain contact with the hot wall beneath the main part of the film, which has already separated from the wall. The subfilm was undergoing dryout due to the formation of random dry patches, while being continuously supplied by liquid from the upstream boiling film near the point of separation. Furthermore, a few droplets seemed at times to be ejected from the separated film onto the hot wall. Upon increasing the heater power, the dry patches occurred more frequently and spread out over a larger fraction of the heated surface area. Just after inception of CHF, Fig. 4(8), the subfilm had evaporated completely, leaving a dry heater surface. The photographs failed to capture the development of the subfilm, which was visible to the naked eye only from a small viewing angle.

To better understand film separation prior to CHF, side view photographs were also obtained for successive power increments. During the earlier stages of film development, side view photography revealed increased waviness and thickening of the film due to

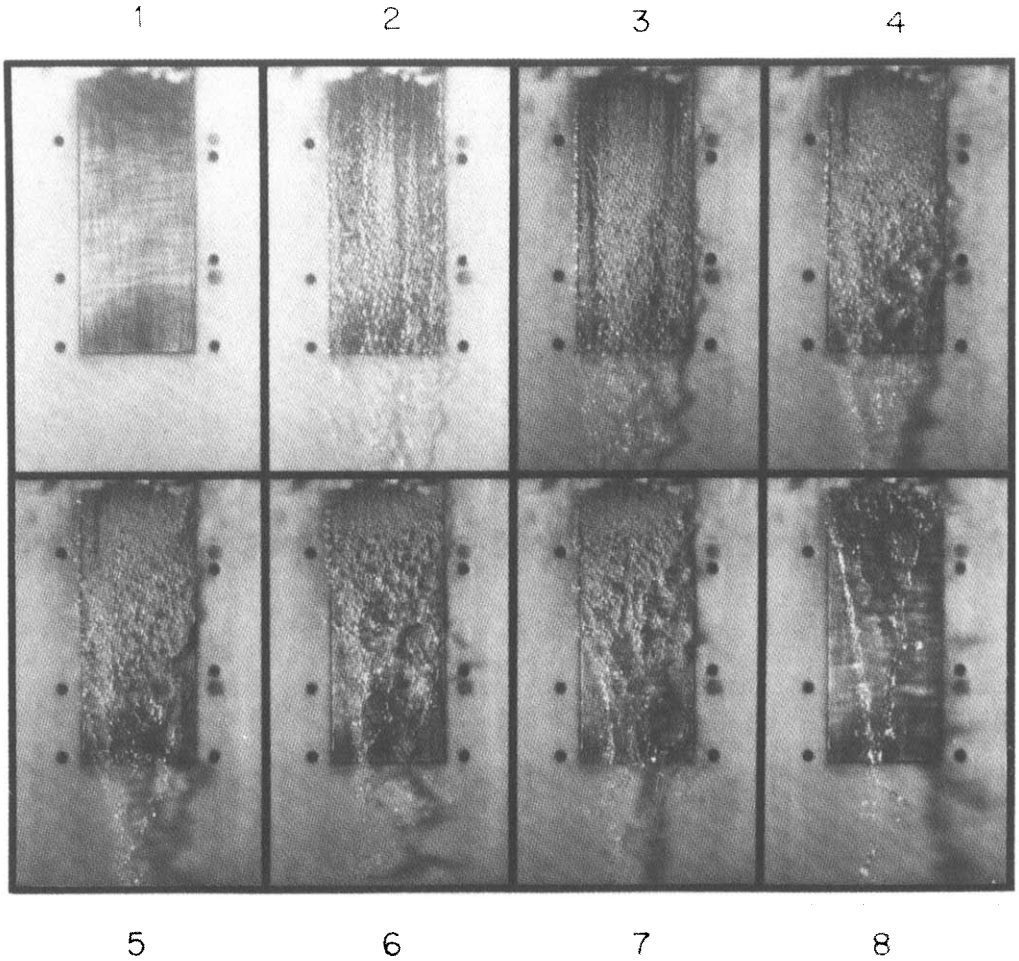

FIG. 4. Front views of successive stages of film development leading to CHF for $U = 0.59\,\text{m s}^{-1}$, $\delta = 0.50\,\text{mm}$ and $L = 63.5\,\text{mm}$. The successive power levels are: (1) bare surface, (2) $q/q_M = 0.36$, (3) $q/q_M = 0.54$, (4) $q/q_M = 0.69$, (5) $q/q_M = 0.77$, (6) $q/q_M = 0.88$, (7) $q/q_M = 0.99$, (8) $q/q_M = 1.0$ (after subfilm dryout).

continuous bubble entrainment in the flow direction. As shown in Fig. 5(4), large bubbles occur intermittently at 80% of CHF, causing partial separation of the film near the downstream edge. Above 90% of CHF, Figs. 5(5) and (6), the separation front moved further upstream. In Fig. 5(7), which corresponds to conditions just before CHF, all but the upstream nucleate boiling region of the film had already separated. Nevertheless, adequate cooling of the wall was still possible by the thin subfilm partially visible in Fig. 5(7). The subfilm had already dried out over the downstream 30% of the heater surface when Fig. 5(8) was taken.

Since film breakdown and separation were precursors to CHF, attempts were made to preserve the liquid continuum of the film by increasing the nozzle spacing or by installing elevated walls on either side of the heater. For the same heater and velocity as Fig. 4, the film thickness was increased to 1.50 mm and Fig. 6 shows the film just after the onset of CHF. In the absence of side walls, the successive stages of film development leading to CHF were similar to those of Fig. 4, except that film separation occurred in the form of several liquid streamers, Fig. 6(1), due to the availability of more liquid in the film. As shown in Fig. 6(2), the side walls seemed to hold the edges of the film, which had a tendency to converge towards the middle without the plates. The stabilizing effect of side walls diminished considerably with longer heaters, for which film convergence was more pronounced. However, since CHF increased by less than 10% due to increasing the film thickness or adding the side plates, it may be concluded that the triggering mechanism for CHF is related to surface conditions beneath the separated film.

The effect of heater length on the CHF is shown in Fig. 7 for three heaters ($L = 24.5$, 63.5 and 127.0 mm). Although film separation and convergence towards the center of the heater appears to be more pronounced for the larger heaters, conditions leading to the CHF were fairly similar to the film behavior of Fig. 4(7), where separated liquid streamers still covered most of the heater surface area.

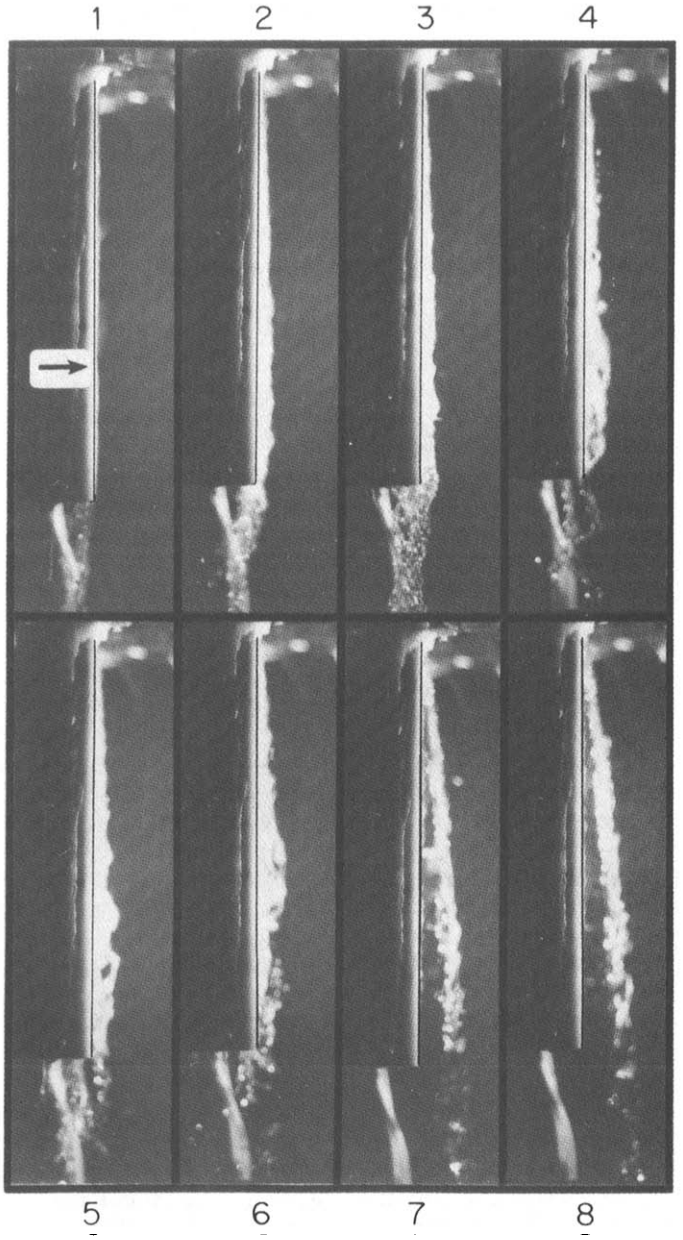

FIG. 5. Side views of successive stages of film development leading to CHF for $U = 0.60\,\mathrm{m\,s^{-1}}$, $\delta = 0.50\,\mathrm{mm}$ and $L = 63.5\,\mathrm{mm}$. The successive power levels are: (1) $q/q_M = 0.0$, (2) $q/q_M = 0.57$, (3) $q/q_M = 0.67$, (4) $q/q_M = 0.80$, (5) $q/q_M = 0.90$, (6) $q/q_M = 0.97$, (7) $q/q_M = 0.99$, (8) $q/q_M = 1.0$ (during subfilm dryout). The arrow shown in the first photograph indicates the lower edge of the heated surface.

EXPERIMENTAL RESULTS

Heat transfer data are presented in the form of boiling curves (wall heat flux vs wall superheat) for different heater lengths, film velocities and nozzle spacings. The heat flux is defined as the total electric power input to the heater module divided by the surface area. Isothermal conditions to within 1°C were maintained along the length of the heater, except for heat fluxes in excess of 95% of CHF, where temperature differences up to 4°C were detected for the 127.0 mm heater. However, in most cases the heater module could be reasonably approximated as an isothermal boundary for the film.

Figures 8 and 9 show the effects of velocity on the boiling characteristics of the film. Prior to boiling, higher velocities increased the heat transfer coefficient and delayed boiling incipience. However, the data generally converged into essentially the same nucleate boiling curve. Boiling hysteresis was practically nonexistent for all operating conditions. Hysteresis is common to FC-72, as previously indicated by other investigators [17, 18]. Bar-Cohen and Simon [19] have indicated that the vanishingly small wetting angle of FC-72 causes flooding and deactivation of potential nucleation sites. Thus excessive surface overheating may be needed to activate these sites. The absence of hysteresis in the present data may be attributed to the

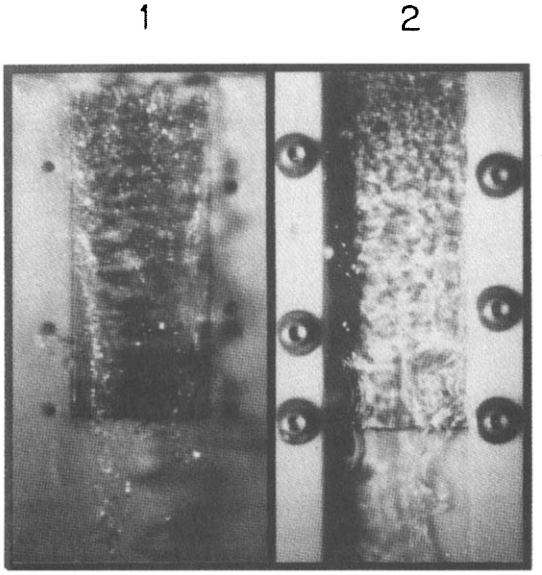

FIG. 6. CHF with and without side walls for $U = 0.55\,\mathrm{m\,s^{-1}}$, $\delta = 1.50\,\mathrm{mm}$ and $L = 63.5\,\mathrm{mm}$

trapping of vapor in cavities, prior to injection of the liquid onto the boiling surface. The insensitivity of the boiling curve to changes in flow velocity indicates that heat transfer in the fully-developed nucleate boiling regime is dominated by bubble activity at the surface, regardless of the contribution of single-phase turbulent transport in the bulk flow. However, the effect of velocity becomes more pronounced at CHF, which is delayed with increasing velocity. This trend is attributed to increased liquid contact with the hot wall and decreased void fraction in the liquid film.

As shown in Fig. 10, the side walls had a small effect on the boiling curve. Furthermore, changes in the CHF resulting from variations of film thickness were not monotonic and seemed to fall within the range of measurement errors (10% of the measured CHF).

As indicated by the flow visualization, the heater length had a significant impact on the boiling characteristics of the film and on CHF. For the same wall flux, the separation caused by bubble entrainment occurs over a relatively short distance for the longer heaters. Thus film breakdown and surface dryout are encountered at lower fluxes in longer heaters. As shown in Fig. 11, CHF for the 12.7 mm heater was roughly twice that of the 127 mm heater for the same nozzle spacing and film velocity.

CHF MODEL FOR SUBCOOLED FALLING LIQUID FILMS

Since it is difficult to interpret all of the individual effects associated with burnout, the analysis will focus on the triggering mechanism for CHF. Flow visualization indicated that, as the heat flux increases, bubbles tend to coalesce in the flow direction and to break down the film near the lower edge of the heater. Just before CHF two phenomena are observed to occur simultaneously: the main part of the film separates completely from the wall and a thin subfilm remains in contact with the wall beneath the separated flow. CHF is then associated with the evaporation and dryout of the subfilm. In this section, these observations are combined in the development of a CHF model.

CHF in many boiling systems has often been attributed to hydrodynamic instabilities associated with the liquid–vapor interface. In his analysis of CHF in pool boiling, Zuber [20] pointed out that, as the bubble population increases at the hot surface, bubbles coalesce and form intermittent vapor blankets. The Taylor instability of the blanket interface results in the effusion of equally-spaced vapor columns. As the heat flux increases, the velocity of vapor jets also increases with respect to the counter current flow of liquid moving towards the surface. Zuber postulated that CHF occurs as a result of the Helmholtz instability, which interrupts the counter current flow and prevents further contact of the liquid with the hot wall. Lienhard and Dhir [21] modified the Taylor–Helmholtz model and developed a new CHF correlation which provided better agreement with experimental data. More recently, Haramura and Katto [16] showed that the driving mechanism for CHF is the Helmholtz instability, which causes several vapor jets to coalesce together and form a massive bubble or blanket in the vicinity of the wall. The Taylor instability affects the size and hovering period of these bubbles near the wall, rather than the size and distribution of the jets. They postulated that CHF occurs when the liquid layer trapped between the bubbles and the wall evaporates completely before the end of the bubble hovering period. Haramura and Katto used the Helmholtz instability alone to successfully model CHF in forced convection boiling on a flat plate and in cross flow over a cylinder.

The proposed model combines the Helmholtz instability concept developed by Zuber with the liquid layer evaporation criterion of Haramura and Katto. The model is based on the assumption that, just before CHF, the vapor jets are rendered hydrodynamically unstable due to the Helmholtz instability and a large vapor blanket is formed. The only remaining source of cooling for the wall is the liquid layer of thickness δ_M equal to the length of the vapor jets. This layer is continuously nourished by incoming liquid from the nozzle. Thus film conditions just before CHF resemble those shown in Fig. 12. As shown in Fig. 5(4), large bubbles occur intermittently in falling films at 80% of CHF, causing only partial separation of the film near the downstream edge of the heater. When the heat flux exceeds 90% of CHF, separation persists at the downstream section and moves further upstream towards the inlet nozzle. This indicates that the liquid subfilm is formed by the propagation of the Helmholtz

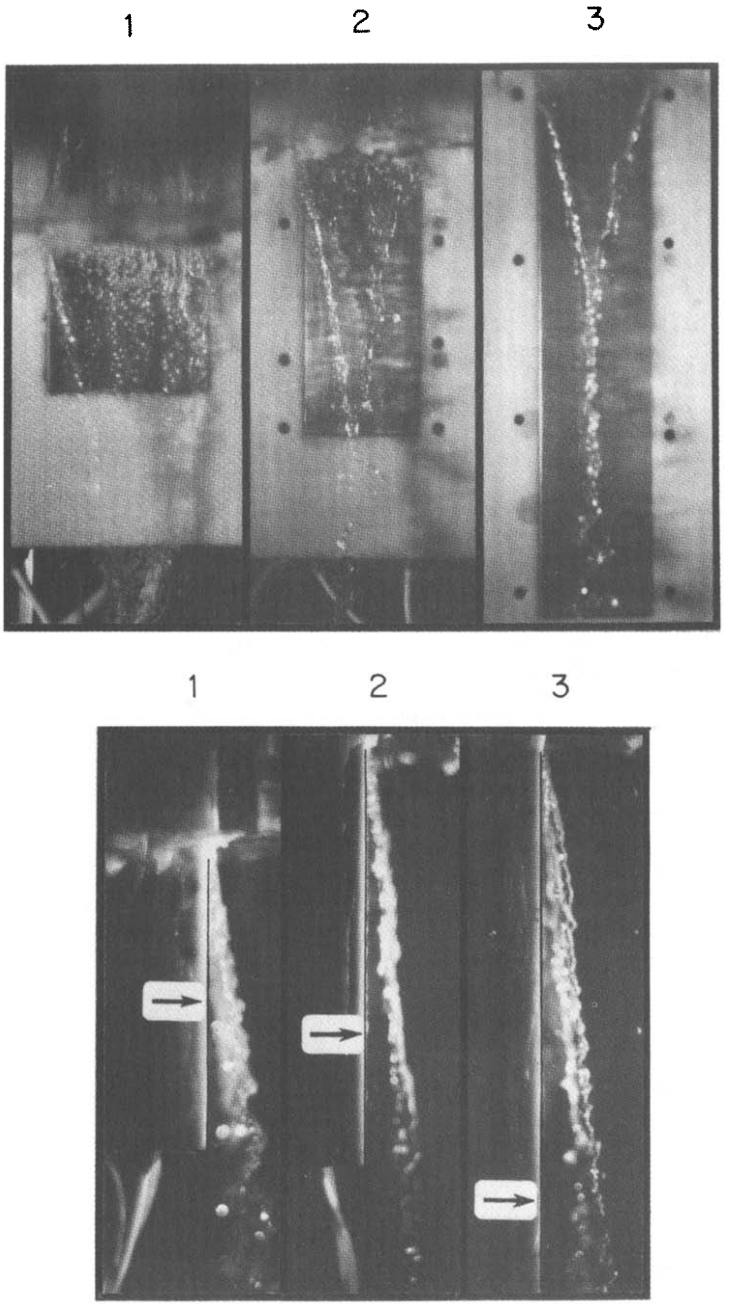

FIG. 7. Effect of heater length on CHF: (1) $L = 25.4$ mm, (2) $L = 63.5$ mm and (3) $L = 127.0$ mm. Arrows shown on each side view indicate the lower edge of the heater surface.

instability towards the inlet section after the heat flux is increased to a value within 90–100% of CHF. In the proposed model the heat flux q, which results in the formation of the subfilm after complete flow separation, is assumed equal to the heat flux necessary for total dryout of the subfilm, q_M.

Before the onset of the Helmholtz instability, the vapor jets leave the surface at velocity u_g in counter current flow with respect to the liquid, which approaches the surface at velocity u_f. Mass conservation between the two phases gives

$$\rho_g u_g A_g = \rho_f u_f (A - A_g) \tag{3}$$

where A_g is the total cross-sectional area of the vapor jets and A is the total surface area. Assuming that all the heat transfer from the wall is converted into latent energy by evaporation of the incoming liquid, the velocity of the vapor jets can be obtained from the energy balance

$$qA = \rho_g u_g A_g h_{fg}. \tag{4}$$

The Helmholtz instability occurs when the relative velocity between the two phases satisfies the criterion

$$|u_g - (-u_f)|^2 \geqslant \frac{2\pi\sigma(\rho_f + \rho_g)}{\rho_f \rho_g \lambda_H} \tag{5}$$

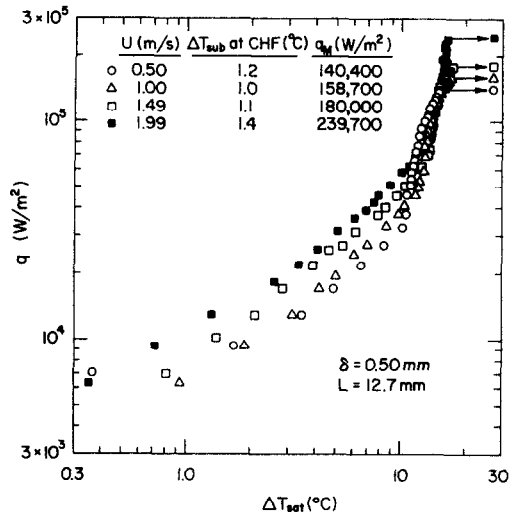

FIG. 8. Effect of velocity on the boiling curve for $L = 12.7$ mm.

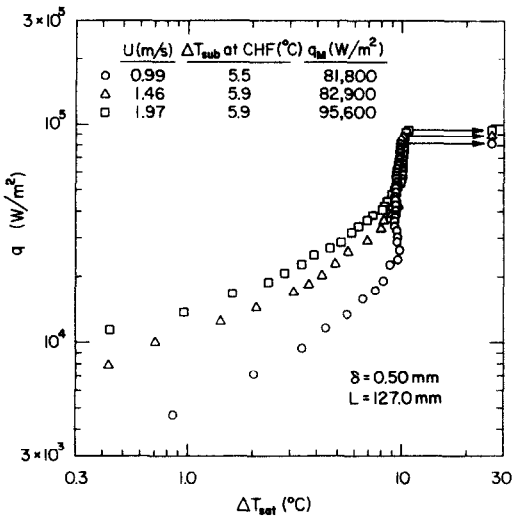

FIG. 9. Effect of velocity on the boiling curve for $L = 127.0$ mm.

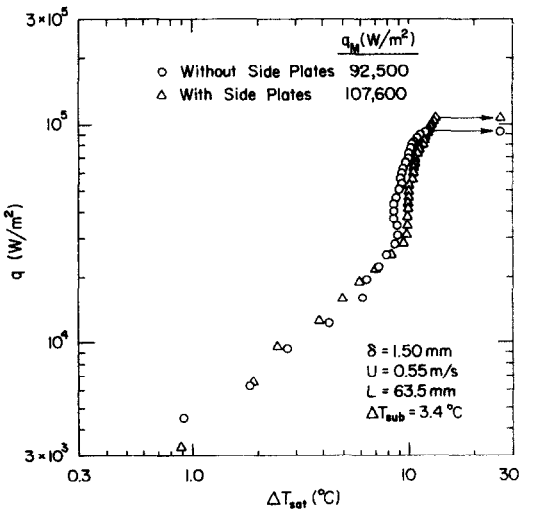

FIG. 10. Effect of side walls on the boiling curve.

where λ_H is the critical wavelength for instability. The maximum thickness δ_M of the liquid layer formed by the collapse of vapor jets is proportional to and of the order of λ_H. Combining equations (3)–(5) yields the following relationship for δ_M

$$\delta_M = 2\pi C_\lambda \left(1+\frac{\rho_g}{\rho_f}\right)\left[\frac{\frac{A_g}{A}}{1+\frac{\rho_g}{\rho_f}\frac{\frac{A_g}{A}}{1-\frac{A_g}{A}}}\right]^2 \frac{\sigma}{\rho_g\left(\frac{q}{\rho_g h_{fg}}\right)^2} \tag{6}$$

where C_λ is a constant of the order of unity.

CHF is postulated to occur when the latent energy of the incoming liquid which penetrates the thin layer equals the total heat supplied at the wall. That is

$$q_M L = \rho_f U \delta_M h_{fg}. \tag{7}$$

Introducing the expression for δ_M in equation (7) gives

$$\frac{q_M/\rho_g h_{fg}}{U} = \psi^{1/3}\left(\frac{\rho_f}{\rho_g}\right)^{2/3}\left(\frac{\sigma}{\rho_f U^2 L}\right)^{1/3} \tag{8}$$

where

$$\psi \equiv 2\pi C_\lambda \left(1+\frac{\rho_g}{\rho_f}\right)\left[\frac{\frac{A_g}{A}}{1+\frac{\rho_g}{\rho_f}\frac{\frac{A_g}{A}}{1-\frac{A_g}{A}}}\right]^2. \tag{9}$$

Since under normal operating conditions $\rho_g/\rho_f \ll 1$, equation (8) simplifies to

$$\frac{q_M/\rho_g h_{fg}}{U} = \left[(2\pi C_\lambda)^{1/3}\left(\frac{A_g}{A}\right)^{2/3}\right]\left(\frac{\rho_f}{\rho_g}\right)^{2/3}\left(\frac{\sigma}{\rho_f U^2 L}\right)^{1/3}. \tag{10}$$

Although ψ is a constant for the conditions of this study, it is not a constant near the critical pressure, which may explain the previously discussed differences in Katto and Shimizu's [11] jet impingement CHF correlations due to pressure variations.

The ratio A_g/A is assumed to be a constant or at best, a weak function of pressure. Zuber [20] and Lienhard and Dhir [21] assumed $A_g/A = \pi/16$, since the diameter of the vapor jets was prescribed by the Taylor instability. Haramura and Katto [16], on the other hand, obtained the expression $A_g/A = 0.0584(\rho_g/\rho_f)^{0.2}$ by equating their relationship for CHF in pool boiling to Zuber's original equation. However, this assumption cannot be generalized to flow boiling applications. In any case, such variations of A_g/A would not have a strong impact on CHF. This

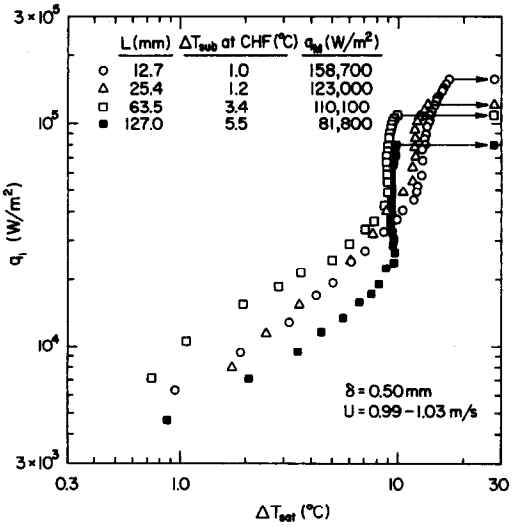

FIG. 11. Effect of heater length on the boiling curve.

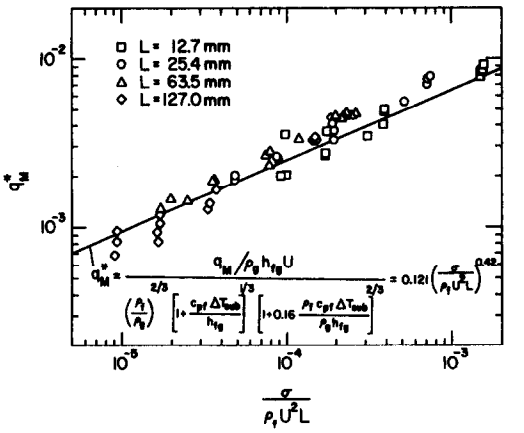

FIG. 13. Comparison of CHF correlation with falling film data.

is evidenced by the resemblance between equation (10) and the empirical correlation of Katto and Ishii for boiling jets

$$\frac{q_M/\rho_g h_{fg}}{U} = 0.0164\left(\frac{\rho_f}{\rho_g}\right)^{0.867}\left(\frac{\sigma}{\rho_f U^2 L}\right)^{1/3}. \quad (11)$$

The proposed CHF model may be extended to include slightly subcooled films. Photographs taken in the present study with subcooled inlet conditions revealed that, prior to CHF, nucleate boiling occurred even at the upstream edge of the heater. This implies that non-equilibrium conditions prevailed across the film and that heat was transferred by bubble effusion and sensible heat exchange in the wall region, rather than by direct sensible heating of the bulk film in the flow direction. Since the 'suction' of subcooled liquid from the bulk of the flow is achieved by the bubble–liquid exchange mechanism, a discrete volume of vapor released by the jets into the bulk region induces an equal volume of subcooled liquid towards the wall. Since the ratio of sensible heat added to the liquid to the latent heat of the released vapor is $\rho_f c_{pf}\Delta T_{sub}/\rho_g h_{fg}$, equation (4) may be rewritten as

$$qA = \rho_g u_g A_g h_{fg}\left[1 + C_{sub}\frac{\rho_f c_{pf}\Delta T_{sub}}{\rho_g h_{fg}}\right] \quad (12)$$

where C_{sub} is a constant smaller than unity. The dryout criterion of equation (7) should also be modified to account for the sensible heat content of the incoming liquid. That is

$$q_M L = \rho_f U \delta_M (h_{fg} + c_{pf}\Delta T_{sub}). \quad (13)$$

Thus inlet subcooling modifies the critical heat flux, such that

$$\frac{q_{M,sub}}{q_{M,sat}} = \left[1 + \frac{c_{pf}\Delta T_{sub}}{h_{fg}}\right]^{1/3}\left[1 + C_{sub}\frac{\rho_f c_{pf}\Delta T_{sub}}{\rho_g h_{fg}}\right]^{2/3} \quad (14)$$

where $q_{M,sat}$ is given by equation (10).

Equation (14) is tested in Fig. 13 against experimental data obtained in the present study. Good agreement between the CHF data and the predictions is obtained for $\psi^{1/3} = 0.121$ and $C_{sub} = 0.16$, but for a Weber number exponent of -0.42 rather than -0.33. That is

$$\frac{q_M/\rho_g h_{fg}}{U} = 0.121\left(\frac{\rho_f}{\rho_g}\right)^{2/3}\left(\frac{\sigma}{\rho_f U^2 L}\right)^{0.42} \times \left[1 + \frac{c_{pf}\Delta T_{sub}}{h_{fg}}\right]^{1/3}\left[1 + 0.16\frac{\rho_f c_{pf}\Delta T_{sub}}{\rho_g h_{fg}}\right]^{2/3} \quad (15)$$

where the experimental ranges for the subcooling

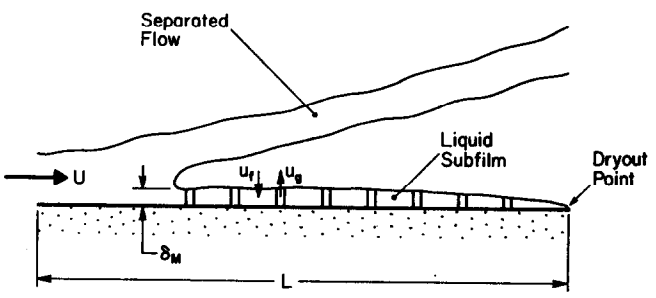

FIG. 12. Schematic representation of the onset of CHF.

terms $c_{pf}\Delta T_{sub}/h_{fg}$ and $(\rho_f/\rho_g)c_{pf}\Delta T_{sub}/h_{fg}$ are 0.00676–0.129 and 0.808–11.53, respectively.

Equation (15) correlates CHF data with a mean accuracy of 18.2% and is recommended for the boiling of vertical liquid films. The difference between the Weber number dependence of the CHF model and that of the experimental correlation may be due to secondary effects, such as partial dryout near the sides and the downstream edge of the heated surface, especially for the longer heaters. The predicted Weber number exponent is identical to that of Katto and Ishii's correlation, equation (11), for high speed wall jets. Their study was conducted with shorter heaters and much higher velocities, which helped prevent partial dryout.

Since the present experiments were conducted at pressures close to atmospheric, the ratio ρ_g/ρ_f is fixed (approximately 0.0083) and the data cannot be used to verify the exponent of 2/3 which appears with the density ratio in equation (15). From previous studies of CHF in thin parallel liquid jets [15], which encompassed density ratios between 0.0006 and 0.005, the exponent of ρ_f/ρ_g was determined empirically to be 0.81 or 0.867 (see equation (11)). If these exponents were used instead of 2/3 in equation (15), the constant coefficient of the present correlation becomes 0.061 or 0.046, respectively. However, from experiments on radial films formed by jet impingement [15] which encompassed the range of density ratios from 0.006 to 0.04, an empirical exponent of 0.645 was determined for ρ_f/ρ_g. This result is in good agreement with the value predicted by the model of this study.

CONCLUSIONS

(1) Nucleate boiling in vertical liquid films causes significant longitudinal variations in film behavior. Vigorous boiling destroys the liquid continuum of the film near the downstream edge of the heater and results in the formation of individual liquid streamers and droplets.

(2) Film breakdown and separation occur prior to CHF. The difference in film behavior for conditions just before and after CHF is the dryout of a thin subfilm beneath the separated liquid.

(3) The film thickness and side walls alter the breakdown pattern of the separated liquid without affecting wall conditions beneath the film. Thus CHF is approximately independent of these two effects.

(4) Higher CHF was achieved with higher film speeds and shorter heaters. Higher velocities also increased the convective heat transfer coefficient prior to boiling and delayed boiling incipiences.

(5) CHF in flowing liquid films is triggered by the Helmholtz instability, which separates the main part of the film leaving a thin liquid layer in contact with the wall. Burnout occurs when the latent heat of the liquid entering this layer at the nozzle is less than the total heater power. A model based on these mechanisms was shown to successfully correlate CHF data.

Acknowledgement—Support by the Data Systems Division of IBM is gratefully acknowledged.

REFERENCES

1. R. Mesler, Nucleate boiling in thin liquid film. In *Boiling Phenomena* (Edited by S. Van Stralen and R. Cole), Vol. 2, pp. 813–819. Hemisphere, Washington (1976).
2. Y. Hsu and R. Graham, *Transport Processes in Boiling and Two-phase Systems*, p. 59. McGraw-Hill, New York (1976).
3. M. G. Cooper, The microlayer and bubble growth in nucleate pool boiling, *Int. J. Heat Mass Transfer* **12**, 915–933 (1969).
4. H. J. Van Ouwerkerk, The rapid growth of a vapour bubble at a liquid–solid interface, *Int. J. Heat Mass Transfer* **14**, 1415–1431 (1971).
5. T. Ueda, M. Inoue and S. Nagatome, Critical heat flux and droplet entrainment rate in boiling of falling liquid films, *Int. J. Heat Mass Transfer* **24**, 1257–1266 (1981).
6. S. Toda and H. Uchida, Study of liquid film cooling with evaporation and boiling, *Trans. Jap. Soc. Mech. Engrs* **38**, 1830–1848 (1972).
7. Y. Katto and M. Kunishiro, Study of the mechanism of burn-out in boiling systems of high burn-out heat flux, *Bull. Jap. Soc. Mech. Engrs* **16**, 1357–1366 (1973).
8. Y. Katto and M. Monde, Study of mechanism of burn-out in high heat-flux boiling system with an impinging jet, *Proc. 5th Int. Heat Transfer Conf.*, Tokyo, Japan, Vol. 4, pp. 245–249 (1974).
9. Y. Katto and K. Ishii, Burnout in a high heat flux boiling system with a forced supply of liquid through a plane jet, *Proc. 6th Int. Heat Transfer Conf.*, Toronto, Canada, Vol. 1, pp. 435–440 (1978).
10. M. Monde and Y. Katto, Burnout in high heat-flux boiling system with an impinging jet, *Int. J. Heat Mass Transfer* **21**, 295–305 (1978).
11. Y. Katto and M. Shimizu, Upper limit of CHF in the saturated forced convection boiling on a heated disk with a small impinging jet, *J. Heat Transfer* **101**, 265–269 (1979).
12. R. P. Baines, M. A. El-Masri and W. M. Rohsenow, Critical heat flux in flowing liquid films, *Int. J. Heat Mass Transfer* **27**, 1623–1629 (1984).
13. J. H. Lienhard and R. Eichhorn, On predicting boiling burnout for heaters cooled by liquid jets, *Int. J. Heat Mass Transfer* **22**, 774–776 (1979).
14. J. H. Lienhard and Md. M. Hasan, On predicting boiling burnout with the mechanical energy stability criterion, *J. Heat Transfer* **101**, 276–279 (1979).
15. Y. Katto, Critical heat flux, *Adv. Heat Transfer* **17**, 1–64 (1985).
16. Y. Haramura and Y. Katto, A new hydrodynamic model of critical heat flux applicable widely to both pool and forced convection boiling on submerged bodies in saturated liquids, *Int. J. Heat Mass Transfer* **26**, 389–399 (1983).
17. A. E. Bergles and M. C. Chyu, Characteristics of nucleate pool boiling from porous metallic coatings, *J. Heat Transfer* **104**, 279–285 (1982).
18. P. J. Marto and V. J. Lepere, Pool boiling heat transfer from enhanced surfaces to dielectric fluids, *J. Heat Transfer* **104**, 292–299 (1982).
19. A. Bar-Cohen and T. W. Simon, Wall superheat excursions in the boiling incipience of dielectric fluids. In *Heat Transfer in Electronic Equipment* (Edited by A. Bar-Cohen), HTD-Vol. 57, pp. 83–94 (1986).
20. N. Zuber, Hydrodynamic aspects of boiling heat transfer, AEC Report No. AECU-4439 (1959).
21. J. H. Lienhard and V. K. Dhir, Hydrodynamic predictions of peak pool-boiling heat fluxes from finite bodies, *J. Heat Transfer* **95**, 152–158 (1973).

TRANSFERT THERMIQUE PAR EBULLITION ET FLUX THERMIQUE CRITIQUE DANS LES FILMS LIQUIDES TOMBANT SUR DES SOURCES MONTEES VERTICALEMENT

Résumé—Des mesures de transfert thermique par ébullition sont obtenus avec un fluorocarbone inerte (FC-72) injecté en film liquide sur une paroi verticale chauffée. Une visualisation montre qu'une ébullition intense avant l'assèchement rompt la continuité du film, causant ainsi la séparation de la plupart du film et laissant un sous-film liquide mince qui maintient le contact avec la paroi. Le flux thermique critique (CHF) est accompagné par l'assèchement du sous-film après séparation totale du liquide près du bord du chauffoir. Un CHF plus élevé est obtenu en augmentant la vitesse du film ou en utilisant un chauffoir plus court. Des données expérimentales se regroupent bien avec les prédictions d'un modèle de CHF basé sur l'instabilité de Helmholtz et la séchage du sous-film.

WÄRMEÜBERGANG BEIM SIEDEN UND KRITISCHE WÄRMESTROMDICHTE IN FLÜSSIGEN FALLFILMEN AN SENKRECHTEN HEIZFLÄCHEN

Zusammenfassung—Es wurden Messungen zum Wärmeübergang beim Sieden eines trägen, über einer vertikalen beheizten Wand verteilten Fluorcarbon (FC-72)-Flüssigkeitsfilms durchgeführt. Die Sichtbarmachung der Strömung zeigte, daß lebhaftes Sieden vor dem "burnout" den zusammenhängenden Flüssigkeitsfilm unterbrach und den größten Teil des Films veranlaßte, sich von der beheizten Wand zu trennen. Dabei bleibt eine dünne Flüssigkeitsunterschicht mit Wandkontakt zurück. Die kritische Wärmestromdichte (CHF) ist verbunden mit dem Austrocknen der Unterschicht nach der vollständigen Verdrängung der Flüssigkeit in der Nähe der Oberkante der Heizfläche. Ein höheres CHF wurde durch Erhöhung der Filmgeschwindigkeit oder durch eine kürzere Heizfläche erreicht. Die experimentellen Daten werden mit einem CHF-Modell, das auf der Helmholtz-Instabilität und Unterschichtaustrocknung beruht, recht gut wiedergegeben.

ТЕПЛООБМЕН ПРИ КИПЕНИИ И КРИЗИС КИПЕНИЯ В ПЛЕНКЕ ЖИДКОСТИ, СТЕКАЮЩЕЙ ПО ВЕРТИКАЛЬНОМУ ТЕПЛОВЫДЕЛЯЮЩЕМУ ЭЛЕМЕНТУ

Аннотация—Проведены измерения теплообмена при пленочном кипении инертного фтороуглерода FC-72 на вертикально нагреваемой стенке. Визуализация потока показала, что интенсивное кипение, предшествующее кризису, нарушало сплошность жидкости и вызывало отделение большей части пленки, так что на ее поверхности оставался тонкий подслой. При достижении критического теплового потока исчезал и этот подслой. Увеличение критического теплового потока было получено за счет повышения скорости стекания пленки или применения более короткого нагревателя. Найдено, хорошее соответствие между экспериментальными данными и результатами расчетов, основанных на модели неустойчивости Гельмгольца при высыхании пленки.